

Active disturbance rejected predictive functional control for space vehicles with RCS

TIAN Jiayi and ZHANG Shifeng*

College of Aerospace Science and Engineering, National University of Defense Technology, Changsha 410073, China

Abstract: Reaction control system (RCS) is a powerful and efficient actuator for space vehicles attitude control, which is typically characterized as a pulsed unilateral effector only with two states (off/on). Along with inevitable internal uncertainties and external disturbances in practice, this inherent nonlinear character always hinders space vehicles autopilot from pursuing precise tracking performance. Compared to most of pre-existing methodologies that passively suppress the uncertainties and disturbances, a design based on predictive functional control (PFC) and generalized extended state observer (GESO) is firstly proposed for three-axis RCS control system to actively reject that with no requirement for additional fuel consumption. To obtain a high fidelity predictive model on which the performance of PFC greatly depends, the nonlinear coupling multiple-input multiple-output (MIMO) flight dynamics model is parameterized as a state-dependent coefficient form. And based on that, a MIMO PFC algorithm in state space domain for a plant of arbitrary orders is deduced in this paper. The internal uncertainties and external disturbances are lumped as a total disturbance, which is estimated and cancelled timely to further enhance the robustness. The continuous control command synthesised by above controller-rejector tandem is finally modulated by pulse width pulse frequency modulator (PWPF) to on-off signals to meet RCS requirement. The robustness and feasibility of the proposed design are validated by a series of performance comparison simulations with some prominent methods in the presence of significant perturbations and disturbances, as well as measurement noise.

Keywords: reaction control system (RCS), predictive functional control (PFC), generalized extended state observer (GESO), pulse width pulse frequency (PWPF), multiple-input multiple-output (MIMO).

DOI: 10.21629/JSEE.2018.05.13

1. Introduction

Since aerodynamic surface control works inefficiently in exoatmospheric flight due to rarefied air, the space vehicles attitude control mainly depends on the reaction control system (RCS) with the advantages of low-cost, high

reliability, and fast response. Over the years, RCS has been applied to space vehicles as diverse as Apollo command module [1], upper stage [2], satellite [3], space shuttle [4], reentry vehicle [5], and space explorer [6].

In general, RCS thrusters can be characterized as pulsed unilateral control effectors only with two states (off/on) [7]. With the RCS actuator, the dynamics of the space vehicles presents strong nonlinearity. Even in circumstances where linear approximations are valid, the utilization of RCS pulse operated thrusters as actuators results in the system that is still inherently nonlinear [8]. In addition, when large angle and/or fast angular slew maneuvers are performed, multi-axis coupling is no longer weak and should be paid special attention to in the design of space vehicles attitude control system. To tackle these intractable problems, extensive studies have been carried out, such as NASA's studying on the Mars Science Laboratory entry vehicle [9] and crew exploration vehicle [10]. And pioneers have suggested mainly two kinds of approaches with respect to this hot topic, which will be surveyed briefly below.

Historically, the single-axis phase-plane analysis method has been proven to be a powerful and effective approach and applied to practical applications [2–6]. This technique establishes empirical switching curves which reflect the error state vectors of the attitude and the attitude rate when switching from one state to another with two assumptions that the equations of motion are uncoupled and the rotation rates are relatively small [8]. Based on this method, many related designs were developed, such as Bang-Bang controller and Bang-off-Bang controller [11], which take the state, control variable, and final state error as penalization items into consideration and provide an recursive or analytical solution using the Pontryagin minimum principle. Since this kind of method is only applicable to the single-axis plant, the model of space vehicles has to be decoupled and linearized in advance. Whereas, these prerequisite cannot always hold and the

control performance would significantly deteriorate especially when large angle and/or fast angular slew maneuvers are required. Note that the above methods directly generate on-off control commands which can be readily implemented by RCS thrusters, so the first kind of methods can be named as the direct method. Compared with that, another kind of method or called indirect method possesses an interpreter or modulator, such as pseudo-rate modulator [12], integral-pulse frequency modulator [13], pulse width modulator [14], and pulse width pulse frequency modulator [15], within their framework, which converts the continuous control command into pulse command sequences to the RCS thrusters by adjusting pulse width and/or pulse frequency according to the level of input. A prominent advantage of such approaches is that more sophisticated methodologies can be applied to address this intractable problem.

It is worth pointing out that most pre-existing methods, both the direct method and the indirect method, are developed based on the nominal plant without considering any external disturbances or parametric perturbations. Nevertheless, time-varying inertia properties, structural and thruster parametric perturbations, installation errors, measurement noise, unmodeled dynamics, and unknown external disturbances (including gravity gradient, magnetic torque, solar radiation pressure, etc.) are always inevitable in practice. As a consequence, the nominal or the best control performance of these controller cannot hold in reality. Especially when encountered uncertainties and disturbances are beyond the inherent robustness authority of these passive disturbance rejection controllers, the deterioration in attitude control performance cannot be tolerant for space vehicles in precise pointing and tracking applications. And what is worse is that little attention has been paid to this research realm.

A robust, exponentially convergent pulse-mode controller for spacecrafts mounted on pulse-operated thrusters was developed in [8]. With the assistance of Lyapunov function, the desired performance is guaranteed even in the presence of modeling errors, unmodeled disturbances and sensor errors. However, strong robustness is achieved for this controller at a price of sacrificing the nominal control performance. Similarly, the same conundrum was encountered by the H_2/H_∞ feedback controller designed in [16]. In [17], a nonlinear finite-time sliding mode control (SMC) controller was proposed for reentry vehicles against external disturbances and parametric perturbations. Although SMC technique is well recognized as one of the most promising robust control techniques, its application is always obstructed by the chattering phenomenon, which leads to oscillation and control accuracy decline, even actuators damage. On the other hand, the performance and

robustness of SMC controllers depend on sliding mode manifold while an ingenious manifold design heavily relies on the designers' empirical knowledge. Therefore, a sophisticated but complicated SMC controller may not be applicable to engineering application from an engineer perspective. Herein, a design based on predictive functional control (PFC) and generalized extended state observer (GESO) is firstly proposed for space vehicles with RCS in this paper. Compared to pre-existing methodologies, this design focuses on actively rejecting rather than passively suppressing the "total disturbance" that includes internal perturbations, unmodeled dynamics, and external disturbances encountered in practice, which not only enhances the robustness of the design but also retains the nominal control performance in the presence of uncertainties and disturbances.

PFC proposed by Richalet [18] in the 80s of last century is the third generation of model predictive control (MPC). MPC has been widely used in the process control realm, and recently is introduced to applications of RCS control system [19,20]. Whereas, a widely recognized shortcoming of MPC is its huge computational burden for online optimization, which makes MPC only applicable to applications with low dynamics where the sample time is measured in seconds or minutes in general [21,22]. Different from solving an optimization problem by online iteration for full MPC, PFC gives a simple analytic optimal solution, which greatly offloads the online computational burden and simultaneously inherits vast majority of merits of full MPC, such as precise tracking [23] and robust stabilization [24]. However, the precondition for satisfying performance of PFC controllers is a sufficiently accurate mathematical predictive model of the plant to be available [25]. Whereas, because of the inevitable internal perturbations and external disturbances, the fidelity of the predictive model cannot be guaranteed. Although the deviation caused by uncertainties can be eliminated partly through the error correction and feedback regulation strategies within the PFC algorithm, this process is usually sluggish or even unstable in the presence of strong uncertainties and disturbances for lacking of penalization items that are directly related to disturbance rejection in the performance index [26]. To access higher fidelity, the predictive model in this paper is parameterized as a multiple-input multiple-output (MIMO) model with state-dependent coefficient (SDC) form for integrated three-axis plant without any Jacobian linearization operation, which preserves all nonlinear and coupling items within the dynamics of the space vehicles.

To accommodate to external disturbances, directly introducing a penalization item into the PFC algorithm seems to be a natural and simple solution but, the control perfor-

mance and robustness of PFC would not be improved significantly because the transformation of the unknown disturbances cannot be precisely predicted in the predictive horizon, for example, the disturbances was just assumed to be constants in the predictive horizon in [27]. Another possible way is to obtain the models of the disturbances in advance by theoretical analysis and then eliminate them in the feedback loop. However, this solution is also infeasible in most cases due to uncertainty and time-variation character of disturbances in practice. The third way would be to estimate and cancel disturbances online to enhance the robustness of PFC controllers with utilizing various disturbance observer, e.g., extended state observer (ESO), linear or nonlinear disturbance observer (DO/NDO), to name a few. In [27], an NDO based PFC controller was investigated for flight vehicles to against significant uncertainties, external disturbances and measurement noise. Liu et al. developed an ESO+PFC controller to regulate the speed of the permanent magnet synchronous motor servo system and received a satisfying performance with fast transient response and good disturbance rejection ability for both the response of simulations and experiments [26]. Indeed, the DO/NDO is a powerful and efficient disturbance observer, but the model of the system should be known in advance. Moreover, the system states cannot be estimated by DO/NDO. Conversely, both disturbances and system states can be synchronously estimated by ESO in an integrated manner while no additional information except system order is required. However, the standard ESO is only applicable to essential integral chain systems subject to matched uncertainties. Fortunately, this intractable problem was solved by GESO proposed in [28]. By appropriately choosing disturbance compensation gain, the GESO-based controller can be directly applied to non-integral chain systems subjected to mismatched uncertainties.

Based on above analyses, a compound controller based on PFC and GESO is proposed herein. The introducing SDC technique guarantees a precise enough predictive model to be available for baseline PFC controller to force the attitude to track the reference signal timely and accurately. All perturbations and disturbances are lumped as a total disturbance, which is estimated by GESO and then directly subtracted from the control input in the feedback loop. Thus, a nominal and disturbance-free model is left for baseline PFC controller design, and the nominal or best control performance could be preserved even under significant parametric perturbations and external disturbances. Finally, the continuous optimal control command synthesised by above controller-rejector tandem is modulated into on-off signals through pulse width pulse frequency (PWPF) modulators.

The remainder of this paper is organized as follows: up-

coming section describes the dynamics model of the space vehicle mounted on RCS. Next, the proposed GESO-PFC-PWPF methodology is introduced in detail. Later, the presented method is applied to the space vehicles autopilot design in the fourth section. Then, the performance comparison simulations with some prominent methods in the presence of disturbances and uncertainties are given in the following section. Finally, some concluding remarks for the paper are presented.

2. Space vehicle dynamics and modeling

The rotational kinematic equations of space vehicles can be described as

$$\dot{\theta} = R(\theta)\omega \quad (1)$$

where $\theta = [\gamma, \psi, \varphi]^T$ is the attitude angle (γ roll angle, ψ yaw angle, and φ pitch angle), attitude angle rate ω is broken up into components along the vehicle body axes as $\omega = [\omega_{x1}, \omega_{y1}, \omega_{z1}]^T$, and

$$R(\theta) = \begin{bmatrix} 1 & \tan \psi \sin \gamma & \tan \psi \cos \gamma \\ 0 & \cos \gamma & -\sin \gamma \\ 0 & \sin \gamma / \cos \psi & \cos \gamma / \cos \psi \end{bmatrix}.$$

Taking the axis coupling into account, the rotational dynamic equations considered herein is

$$I\dot{\omega} = \Omega(\omega)\omega + M + d_0 \quad (2)$$

where M is the control moment. d_0 represents a total disturbance which may include parametric perturbations, unknown disturbance, and unmodeled dynamics, etc. And the moment of inertia matrix I and coupling matrix Ω are

$$I = \begin{bmatrix} I_{xx} & -I_{xy} & -I_{xz} \\ -I_{yx} & I_{yy} & -I_{yz} \\ -I_{zx} & -I_{zy} & I_{zz} \end{bmatrix}$$

$$\Omega(\omega) =$$

$$\begin{bmatrix} I_{zx}\omega_y - I_{yx}\omega_z & I_{zy}\omega_y - I_{zz}\omega_z & I_{yy}\omega_y - I_{yz}\omega_z \\ I_{zz}\omega_z - I_{zx}\omega_x & I_{xy}\omega_z - I_{zy}\omega_x & I_{xz}\omega_z - I_{xx}\omega_x \\ I_{yx}\omega_x - I_{yy}\omega_y & I_{xx}\omega_x - I_{xy}\omega_y & I_{yz}\omega_x - I_{xz}\omega_y \end{bmatrix}.$$

Let $x = [\theta; \omega]$ be the system state, u normalized control command. Combining (1) and (2), the state equation of SDC form for space vehicles dynamics can be described as

$$\dot{x} = A(x)x + B(u + d_0) \quad (3)$$

where

$$A(x) = \begin{bmatrix} 0_{3 \times 3} & R(\theta) \\ 0_{3 \times 3} & I^{-1}\Omega(\omega) \end{bmatrix}, \quad B = \begin{bmatrix} 0_{3 \times 3} \\ I^{-1}M' \end{bmatrix}$$

and M' is a diagonal matrix, whose elements of principal diagonal are ones in M .

The control objective herein is to track reference attitude angle θ_c , thus the output equation is

$$y = Cx \quad (4)$$

where $C = [I_{3 \times 3}, \mathbf{0}_{3 \times 3}]$, and $I_{3 \times 3}$ represents the identity matrix of three order.

Given that θ_c cannot be predicted in the predictive horizon, the tracking problem is converted into regulating problem herein by selecting the system states as $x = [\theta - \theta_c; \omega]$. Accordingly, the states equation and output equation are

$$\begin{cases} \dot{x} = A(x)x + B(u + d_0) + \begin{bmatrix} \dot{\theta}_c \\ \mathbf{0}_{3 \times 3} \end{bmatrix} + A(x) \begin{bmatrix} \theta_c \\ \mathbf{0}_{3 \times 3} \end{bmatrix} \\ y = Cx \end{cases} \quad (5)$$

It should be pointed out that the x in SDC matrix $A(x)$ represents θ and ω not the system state. For the sake of simplicity and clarity, the real $A(\theta, \omega)$ still denotes as $A(x)$ hereinafter.

Note that the last two items are mismatched disturbances. To tackle that, the following lemma from [29] is introduced.

Lemma 1 Let $\Phi = \{p_i \sin(\omega_i t + \phi_i)\}$, $i = 0, 1, \dots, n, n < \infty$, where $\omega_i (\geq 0)$ and ϕ_i are constants, p_i denotes any polynomials at time t .

Suppose the linear system

$$\begin{cases} \dot{x} = Ax + Bu + B_d d \\ y = Cx \end{cases} \quad (6)$$

is controllable and observable, and has no zeros on the imaginary axis. If its output y_1 for the disturbance d belongs to Φ , then, from the concept of stable inversion[30], it follows that there exists a system:

$$\begin{cases} \dot{\bar{x}} = A\bar{x} + B(u + d_e) \\ \bar{y} = C\bar{x} \end{cases} \quad (7)$$

whose output \bar{y}_1 for the disturbance d_e satisfies $\bar{y}_1 \equiv y_1$ for all $t \geq 0$. The disturbance d_e that acts via the same channel as the control input is called the equivalent input disturbance (EID) for the disturbance d . And the system (7) is called the EID system for the original system (6).

Assumption 1 $(A(x), B)$ is controllable, and $(\bar{A}(x), \bar{C})$ is observable at any sampling time.

In practice, almost most output of practical system belongs to Φ , then there always exists an EID system for that [31]. Consequently, the system (5) can be further written as an EID system under the Assumption 1 as

$$\begin{cases} \dot{x} = A(x)x + B(u + d) \\ y = Cx \end{cases} \quad (8)$$

Remark 1 Essentially, the EID technique can be regarded as a sophisticated coordinate transformation with the aim of guaranteeing the output produced by disturbance invariable. Thus, the system state in system (8) is

no longer the one in the system (5). And because this coordinate transformation is too complicated, the transformed system state and EID will be typically obtained by estimation but not direct calculation.

Hereto, the complex space vehicle dynamics in the presence of parametric perturbations and external disturbance is modeled as a MIMO SDC model (8), which will be used for the control model in the following design.

3. Space vehicle autopilot design

Herein, the controller is composed of three parts: GESO, MPFC (MIMO-PFC), and PWPF modulator. Internal uncertainties (possibly including unmodeled dynamics and parametric perturbations) and external disturbances are treated as a lumped disturbance, which is estimated by GESO. Then the lumped disturbance is directly subtracted from the optimal control command u^* obtained by MPFC controller in the negative feedback loop, i.e., $\bar{u} = u^* - d$. Finally, the continuous control command \bar{u} is discretized by PWPF modulator into on-off signals to meet the demand of RCS effectors. For simplicity, the RCS dynamics is ignored and considered to be ideal in this paper. The configuration of the proposed method for space vehicles autopilot is depicted in Fig. 1.

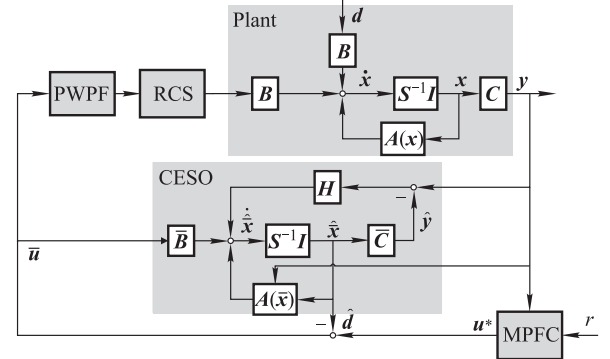


Fig. 1 Configuration of GESO-MPFC-PWPF system

3.1 GESO

In this section, GESO is developed to estimate the transformed system states \hat{x} and EID \hat{d} . Defining extended states $x' = d$, the extended state equation is obtained as

$$\begin{cases} \dot{\bar{x}} = \bar{A}(x)\bar{x} + \bar{B}u + E\dot{d} \\ y = \bar{C}\bar{x} \end{cases} \quad (9)$$

where $\bar{x} = [x; x']$ is the system state, \dot{d} is the rate of change of EID. System matrices are $\bar{C} = [C, \mathbf{0}_{3 \times 3}]$, $\bar{A}(x) = \begin{bmatrix} A(x) & B \\ \mathbf{0}_{3 \times 6} & \mathbf{0}_{3 \times 3} \end{bmatrix}$, $\bar{B} = \begin{bmatrix} B \\ \mathbf{0}_{3 \times 3} \end{bmatrix}$, $E = \begin{bmatrix} \mathbf{0}_{6 \times 3} \\ I_{3 \times 3} \end{bmatrix}$.

Assumption 2 The lumped disturbance meets the following requirements: (i) d is bounded; (ii) \dot{d} has constant mean value in steady state, i.e., $\lim_{t \rightarrow \infty} \dot{d} = \lim_{t \rightarrow \infty} h = \mathbf{0}$.

For system (4), the GESO is designed as

$$\begin{cases} \dot{\hat{x}} = \bar{A}(x)\hat{x} + \bar{B}u + H(y - \hat{y}) \\ \hat{y} = \bar{C}\hat{x} \end{cases} \quad (10)$$

where $\hat{x} = [\hat{x}; \hat{x}']$ is the estimated system state, and H is the observer gain matrix to be designed.

The GESO estimation error vector can be defined as $e = \hat{x} - \bar{x}$. Combining (9) and (10), the estimation error equation is

$$\dot{e} = (\bar{A}(x) - HC)e - Eh. \quad (11)$$

The asymptotical stability of the GESO can be obtained from the following conclusion.

Lemma 2 The following multiple-input linear system

$$\dot{x} = Ax + Bu \quad (12)$$

has a Hurwitz matrix A , then the system (12) is bounded stable for any bounded u . And if u further satisfies $\lim_{t \rightarrow \infty} u = 0$, the system (13) is asymptotically stable.

Proof Suppose that Assumption 2 is satisfied. According to Lemma 2, the asymptotical stability of estimation error e for any bounded h and d at any sampling time is guaranteed if the observer gain matrix H is designed such that $\bar{A}(x) - HC$ is a Hurwitz matrix. \square

3.2 MPFC

An MPFC control for the MIMO plant of the arbitrary order is proposed in this subsection. Given that the EID has been estimated by GESO, the following model is utilized as a control model for MPFC controller design:

$$\begin{cases} \dot{x} = A(x)x + Bu \\ y = Cx \end{cases} \quad (13)$$

3.2.1 Basis function

In the PFC algorithm, control command is assumed to be a weighted sum of the known basis function. At sampling time $k + i$, the control command can be described as

$$u(k+i) = \begin{bmatrix} u_1(k+i) \\ \vdots \\ u_N(k+i) \end{bmatrix} = \begin{bmatrix} \sum_{j=1}^{N_b} \mu_{1j} f_j(i) \\ \vdots \\ \sum_{j=1}^{N_b} \mu_{Nj} f_j(i) \end{bmatrix} = \begin{bmatrix} \mu_{11} & \cdots & \mu_{1N_b} \\ \vdots & \ddots & \vdots \\ \mu_{N1} & \cdots & \mu_{NN_b} \end{bmatrix} \begin{bmatrix} f_1(i) \\ \vdots \\ f_{N_b}(i) \end{bmatrix} \quad (14)$$

where $i = 0, 1, \dots, p-1$. p is the predictive horizon, μ_{nj} is the unknown weighted coefficient of n th control command $u_n(k+i)$ corresponding to the basis function $f_j(\cdot)$,

N_b is the number of the basis functions, and N is the order of the control command.

3.2.2 Predictive model

The discrete predictive model of the system (13) can be described as

$$\begin{cases} x_m(k+1) = A_m x_m(k) + B_m u(k) \\ y_m(k) = C_m x_m(k) \end{cases} \quad (15)$$

where A_m , B_m and C_m are SDC matrices and are expressed as $A_m = e^{A(x)T_s}$, $B_m = \int_0^{T_s} e^{A(x)T_s} B dt$, $C_m = C$. T_s is the discrete period of the predictive model, which is typically equal to the control period.

For (15), its predictive output in the predictive horizon can be obtained by iterating the predictive state. The later at sampling time $k+i$ is

$$x_m(k+i) = A_m^i x_m(k) + \sum_{j=0}^{i-1} A_m^{i-j-1} B_m u(k+j). \quad (16)$$

Then, the predictive output is

$$y_m(k+i) = M(i) + y_f(k+i) =$$

$$C_m A_m^i x_m(k) + \sum_{j=0}^{i-1} C_m A_m^{i-j-1} B_m u(k+j) \quad (17)$$

for $i = 1, 2, \dots, p$.

It is obvious that the predictive output consists of two parts, namely the free output $M(i)$ and the forced output $y_f(k+i)$. $M(i)$ is only related to the previous system state and control input with the hypothesis of $u(k+i) = 0$ ($i \geq 0$). $y_f(k+i)$ is the response to the control command at sampling time $k+i$. Let $C_m A_m^{i-1-j} B_m = N_j$, $j = 1, \dots, i$, $y_f(k+i)$ can be expressed as

$$y_f(k+i) = \begin{bmatrix} \sum_{j=1}^i \sum_{n=1}^N N_j(1,n) u_n(k+j-1) \\ \vdots \\ \sum_{j=1}^i \sum_{n=1}^N N_j(l,n) u_n(k+j-1) \end{bmatrix} \quad (18)$$

where l is the dimension of the system output, $N_j(m,n)$ is the (m,n) entries of the matrix N_j .

Combining (14) and (18), $y_f(k+i)$ is reconstructed as

$$y_f(k+i) = \begin{bmatrix} \sum_{j=1}^i \sum_{n=1}^N \sum_{p=1}^{N_b} N_j(1,n) \mu_{np} f_p(j-1) \\ \vdots \\ \sum_{j=1}^i \sum_{n=1}^N \sum_{p=1}^{N_b} N_j(l,n) \mu_{np} f_p(j-1) \end{bmatrix} \quad (19)$$

Equation (19) is further rewritten as $\mathbf{y}_f(k+i) = \mathbf{K}(i)\mathbf{U}$, where $\mathbf{U}^T = [\mu_{11}, \dots, \mu_{1N_b}, \mu_{21}, \dots, \mu_{NN_b}]$, and the l th row of the $\mathbf{K}(i)$ is

$$\mathbf{K}(i) = \begin{bmatrix} \sum_{j=1}^i N_j(l, 1)f_1(j-1) \\ \vdots \\ \sum_{j=1}^i N_j(l, 1)f_{N_b}(j-1) \\ \sum_{j=1}^i N_j(l, 2)f_1(j-1) \\ \vdots \\ \sum_{j=1}^i N_j(l, N)f_{N_b}(j-1) \end{bmatrix}^T.$$

Thus, the predictive output at sampling time $k+i$ is

$$\mathbf{y}_m(k+i) = \mathbf{M}(i) + \mathbf{K}(i)\mathbf{U}. \quad (20)$$

3.2.3 Error correction

In practice, it is inevitable that errors exist between the predictive and actual outputs. Traditionally, the predictive output error within a prediction horizon is considered as

$$\mathbf{e}(k+i) = \mathbf{y}(k+i) - \mathbf{y}_m(k+i) = \mathbf{y}(k) - \mathbf{y}_m(k) \quad (21)$$

where $\mathbf{y}(k+i)$ is the actual output at sampling time $k+i$.

Then, the predictive output is corrected as

$$\begin{aligned} \mathbf{y}_p(k+i) &= \mathbf{y}_m(k+i) + \mathbf{e}(k+i) = \\ &= \mathbf{y}_m(k+i) + \mathbf{y}(k) - \mathbf{y}_m(k). \end{aligned} \quad (22)$$

3.2.4 Reference trajectory

The reference trajectory regards current system state as the initial state and approaches the designed set-point trajectory in a specified manner. Generally, the exponential function is selected to describe the reference trajectory

$$\mathbf{y}_r(k+i) = \mathbf{y}_c(k+i) - \beta^i(\mathbf{y}_c(k) - \mathbf{y}(k)) \quad (23)$$

where $\mathbf{y}_r(k+i)$ is the reference trajectory at sampling time $k+i$, $\mathbf{y}_c(k+i)$ is the corresponding set-point, $\beta = e^{-T_s/T_r}$ is the softness factor which adjusts the approach ratio of the reference trajectory to the set-point. And T_r represents expected settling time of the reference trajectory.

3.2.5 Performance index

The Euclidean norm of tracking error vectors between reference trajectory and predictive output at several coincidence points is adopted as the performance index, namely

$$J = \sum_{h_i \in H_{N_c}} \|\mathbf{y}_r(k+h_i) - \mathbf{y}_p(k+h_i)\|^2 \quad (24)$$

where the coincidence point $h_i \in H_{N_c} = \{h_1, \dots, h_{N_c}\}$, and N_c is the number of the coincidence points.

3.2.6 Control command calculation

Expand performance index (24)

$$J = \sum_{h_i \in H_{N_c}} \|\mathbf{y}_r(k+h_i) - \mathbf{y}_p(k+h_i)\|^2 = \|\mathbf{L} - \mathbf{R}\mathbf{U}\|^2 \quad (25)$$

where $\mathbf{R}^T = [\mathbf{K}^T(h_1), \dots, \mathbf{K}^T(h_{N_c})]$, and

$$\mathbf{L} = \begin{bmatrix} \mathbf{y}_r(k+h_1) - \mathbf{M}(h_1) - \mathbf{y}(k) + \mathbf{y}_m(k) \\ \vdots \\ \mathbf{y}_r(k+h_{N_c}) - \mathbf{M}(h_{N_c}) - \mathbf{y}(k) + \mathbf{y}_m(k) \end{bmatrix}.$$

In the case of no constraints, the optimal control can be derived by minimizing the performance index J in terms of weighted coefficient vector \mathbf{U} as

$$\mathbf{U} = (\mathbf{R}^T \mathbf{R})^{-1} \mathbf{R}^T \mathbf{L}. \quad (26)$$

Rewriting the optimal weighted coefficient vector \mathbf{U} as

$$\boldsymbol{\mu}^* = \begin{bmatrix} \mu_{11} & \cdots & \mu_{1N_b} \\ \vdots & \ddots & \vdots \\ \mu_{N1} & \cdots & \mu_{NN_b} \end{bmatrix}. \quad (27)$$

Thus, the optimal control is given by

$$\mathbf{u}^* = \boldsymbol{\mu}^* \mathbf{F} \quad (28)$$

where $\mathbf{F} = [f_1, \dots, f_{N_b}]^T$.

3.3 PWPF modulator

Based on GESO-MPFC controller, the continuous optimal control command is obtained as

$$\bar{\mathbf{u}} = \mathbf{u}^* - \mathbf{d}. \quad (29)$$

For space vehicles, the continuous control command has to be modulated by PWPF modulator into on-off signals. In general, a basic PWPF modulator, as shown in Fig. 2, consists of a first-order-filter and a Schmidt trigger. The first-order-filter is defined by arguments K and T and the Schmidt trigger is a simple on-off relay with dead zone and hysteresis.

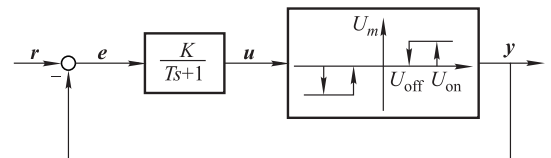


Fig. 2 Configuration of GESO-MPFC-PWPF system

When the positive signal input to the Schmidt trigger is greater than the given U_{on} , the Schmidt trigger outputs U_m ; and when it falls below U_{off} , the Schmidt trigger outputs 0. For negative signals, the output is exactly opposite. The hysteresis of the Schmidt trigger is defined as

$h \triangleq U_{on} - U_{off}$. More detail about PWPF modulator can be found in [32].

The configuration of the GESO-MPFC-PWPF controller is depicted in Fig. 3.

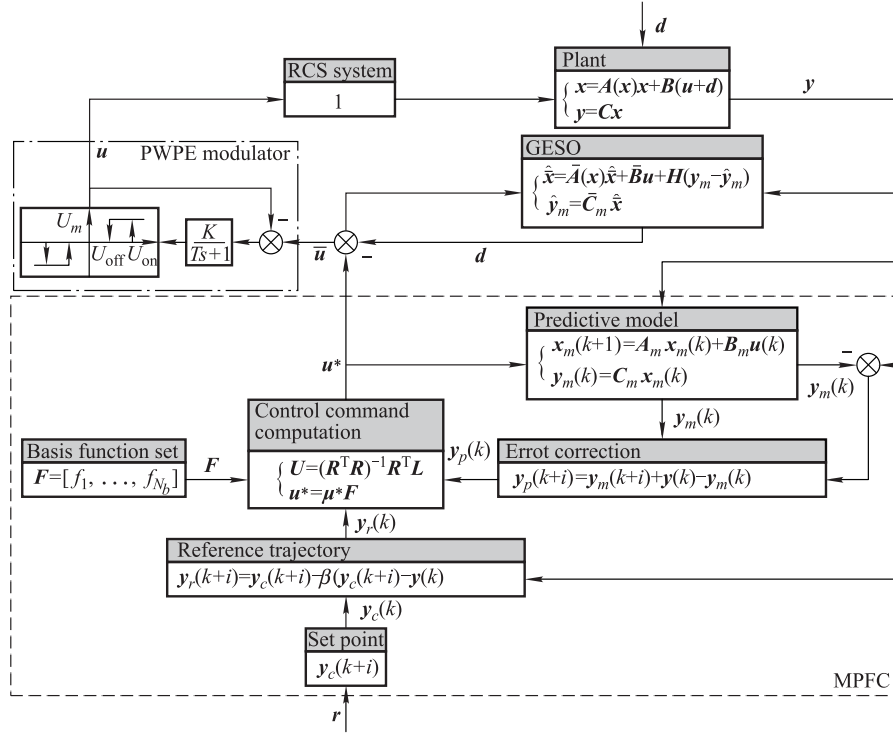


Fig. 3 Configuration of GESO-MPFC-PWPF system

4. Brief introduction for comparison controllers

In order to further study the robustness and superiority of the designed controller, comparison simulations are carried out in this section with some pre-existing designs, including a traditional phase plane controller and a linear quadratic regulator (LQR)-PWPF controller. The former proves effective in engineering application, and the latter proposed by Xu et al. [33] for a kinetic kill vehicle receives favorable performance both in tracking accuracy and fuel consumption. A brief introduction for the two controllers is given in the following.

4.1 Phase plane controller

Decoupling and linearization are first carried out for single-axis phase plane control. According to small perturbation theory, the attitude angle and angle velocity of space vehicle are considered as small quantities. The trigonometric function for the attitude angle is substituted by its approximate form, and the product of small quantities are ignored. Thus, the rotational kinematic equations (1) and

rotational dynamic equations (2) are decoupled and simplified to a three-axis self-governed second-order linear model.

Pitch channel:

$$\begin{cases} \dot{\varphi} = \omega_{z_1} \\ \dot{\omega}_{z_1} = (M_{z_1} + d_{z_1})/I_{z_1} = k_{z_1} u_{z_1} \end{cases} \quad (30)$$

Yaw channel:

$$\begin{cases} \dot{\psi} = \omega_{y_1} \\ \dot{\omega}_{y_1} = (M_{y_1} + d_{y_1})/I_{y_1} = k_{y_1} u_{y_1} \end{cases} \quad (31)$$

Roll channel:

$$\begin{cases} \dot{\gamma} = \omega_{x_1} \\ \dot{\omega}_{x_1} = (M_{x_1} + d_{x_1})/I_{x_1} = k_{x_1} u_{x_1} \end{cases} \quad (32)$$

In (30)–(32), u_i are the normalized control command, k_i is the coefficients corresponding to the control command. Note that this model is also adopted to design LQR-PWPF controller.

Take the pitch channel for example, four switching curves are designed for RCS on-off state on the phase plane, namely,

Negative switching on curve:

$$\varphi + \tau\dot{\varphi} = d \quad (33)$$

Negative switching off curve:

$$\varphi + \tau\dot{\varphi} = d - \delta \quad (34)$$

Positive switching on curve:

$$\varphi + \tau\dot{\varphi} = -d \quad (35)$$

Positive switching off curve:

$$\varphi + \tau\dot{\varphi} = -(d - \delta). \quad (36)$$

In (33)–(36), τ is the slope of the switching curve that represents the damping stability, d is the threshold of RCS thruster boot-strep, and δ is the delay constant of the RCS thruster. According to the switching curve, the control law is

$$u = \begin{cases} -1, & \varphi + \tau\dot{\varphi} \geq d; \dot{\varphi} > 0; \\ & \varphi + \tau\dot{\varphi} \geq d - \delta; \dot{\varphi} < 0 \\ 0, & -(d - \delta) < \varphi + \tau\dot{\varphi} < d; \dot{\varphi} > 0; \\ & -d < \varphi + \tau\dot{\varphi} < d - \delta; \dot{\varphi} < 0 \\ 1, & \varphi + \tau\dot{\varphi} \leq -d; \dot{\varphi} < 0; \\ & \varphi + \tau\dot{\varphi} \leq -(d - \delta); \dot{\varphi} > 0 \end{cases} \quad (37)$$

The schematic diagram of switching curves on the phase plane is depicted in Fig. 4. There is a limit cycle around the origin of the phase plane reflecting the dynamics of the system. The dead zone width and height of limit cycle represent the precision errors of attitude tracking and the operating time of RCS effectors, respectively. In general, the limit cycle is designed as a tabular rectangle for saving propellant, namely, widening the width of the dead zone while decreasing its height. Considering the control precision and on-off times of RCS, the absolute error of attitude tracking is expected not to exceed 0.5° , that is, $d = 0.5$. And according to the simulation, the choice, $\tau = 0.1$ and $\delta = 0.05$, is appropriate. These parameters are applicable to each channel.

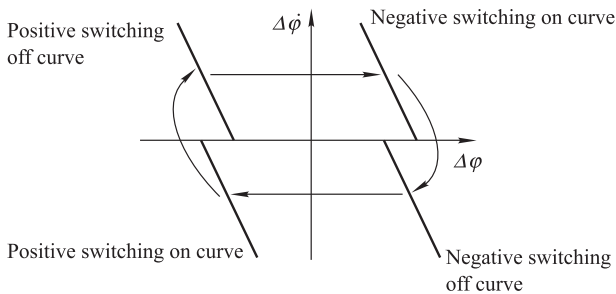


Fig. 4 Switching curves on the phase plane

4.2 LQR-PWPF controller

The dynamics of the space vehicle for three channels (30)–(32) can be expressed in the same form, i.e., a second order system

$$\begin{cases} \dot{\mathbf{x}} = \mathbf{A}\mathbf{x} + \mathbf{B}\mathbf{u} \\ \mathbf{y} = \mathbf{C}\mathbf{x} \end{cases} \quad (38)$$

where $\mathbf{x} = [x_1; x_2]$ is the system state, $\mathbf{y} = [y_1; y_2]$ is the system output, and the system matrices are $\mathbf{B} = [0; 1]$, $\mathbf{A} = \begin{bmatrix} 0 & 1 \\ 0 & 0 \end{bmatrix}$, and $\mathbf{C} = \begin{bmatrix} 1 & 0 \\ 0 & 1 \end{bmatrix}$.

Given the tracking error and fuel consumption, the cost function is defined as

$$J = \frac{1}{2} \int_{t_0}^{t_f} [\mathbf{e}^T(t) \mathbf{Q} \mathbf{e}(t) + \mathbf{u}^T(t) \mathbf{R} \mathbf{u}(t)] dt \quad (39)$$

where $\mathbf{e} = \tilde{\mathbf{y}} - \mathbf{y}$ is the error of the expected output and the real output, \mathbf{Q} is a positive definite matrix and \mathbf{R} is a semi-positive definite matrix. The design of weighting matrices \mathbf{Q} and \mathbf{R} should be a trade-off between tracking performance and control efforts.

The approximate optimal control for the infinity time fixed-length tracking problem is obtained by minimizing J , which is depicted as

$$\hat{\mathbf{u}}(t) = -\mathbf{R}^{-1} \mathbf{B} [\mathbf{P} \mathbf{x} - \mathbf{g}] \quad (40)$$

where \mathbf{P} is a symmetry positive constant matrix that is obtained by solving the Riccati equation

$$\mathbf{P} \mathbf{A} + \mathbf{A}^T \mathbf{P} - \mathbf{P} \mathbf{B} \mathbf{R}^{-1} \mathbf{B}^T \mathbf{P} + \mathbf{C}^T \mathbf{Q} \mathbf{C} = 0.$$

And \mathbf{g} is a constant concomitance vector, which is obtained by the following equation:

$$\mathbf{g} = [\mathbf{P} \mathbf{B} \mathbf{R}^{-1} \mathbf{B}^T - \mathbf{A}^T]^{-1} \mathbf{C}^T \mathbf{Q} \tilde{\mathbf{y}}.$$

In this paper, the selection of the weighting matrices is $\mathbf{Q} = \begin{bmatrix} 100 & 0 \\ 0 & 10 \end{bmatrix}$ and $\mathbf{R} = 0.55$ for three channels.

5. Simulation studies

5.1 Parameters of the space vehicle and controllers

According to [33], the physical parameters of the simulation model are listed in Table 1.

Table 1 Physical parameters of space vehicle system

Parameter	Pitch channel	Yaw channel	Roll channel
Arm of force/m	0.437	0.437	0.240
Moment/N·m	8.74	8.74	4.8
Moment of inertia/kg·m ²	2	2	1
Thruster force/N	20	20	20

The observer gain matrix H in GESO is designed based on pole placement. The poles are 20, 22.5, and 27.5 for pitch channel, yaw channel, and roll channel respectively. For MPFC controller, the basis function is selected as $f_1(\cdot) = 1$. The control period T_s is 10 ms, and the settling time T_r are 0.3 s for roll channel and 0.35 s for yaw and pitch channels. The predictive horizon p is 8, and the set of the coincidence points in the performance index is $H_{N_c} = \{7, 8\}$. The same PWPF modulator is adopted both for the proposed controller (hereinafter referred as GESO-MPFC-PWPF controller) and LQR-PWPF controller, whose parameters are listed in Table 2.

Table 2 PWPF modulator parameters

Parameter	U_{on}	U_{off}	U_m	K	T
Setting	0.8	0.3	1	5	0.05

5.2 Static tracking

The following simulations are implemented on MATLAB/SIMULINK software with the Runge-Kutta integral method with a fixed-step of 10 ms. The step reference signal is selected to verify the static tracking performance for three controllers both in Case I (attitude fine-tuning) and Case II (large angle maneuver). And the initial values of three angular velocities are all zero. The response curves and control command for three controllers are depicted in Fig. 5 and Fig. 6 respectively. For Case I, all three controllers are capable of tracking the reference signal within given accuracy (0.5°). For Case II, to promptly track 60° step reference command, both LQR-PWPF and phase plane controller possess obvious overshoot, especially up to 80° for phase plane controller. Reversely, GESO-MPFC-PWPF controller exhibits satisfying performance in terms of non-overshoot, fast dynamical response (less than 2 s), small steady-state error (less than 0.5°).

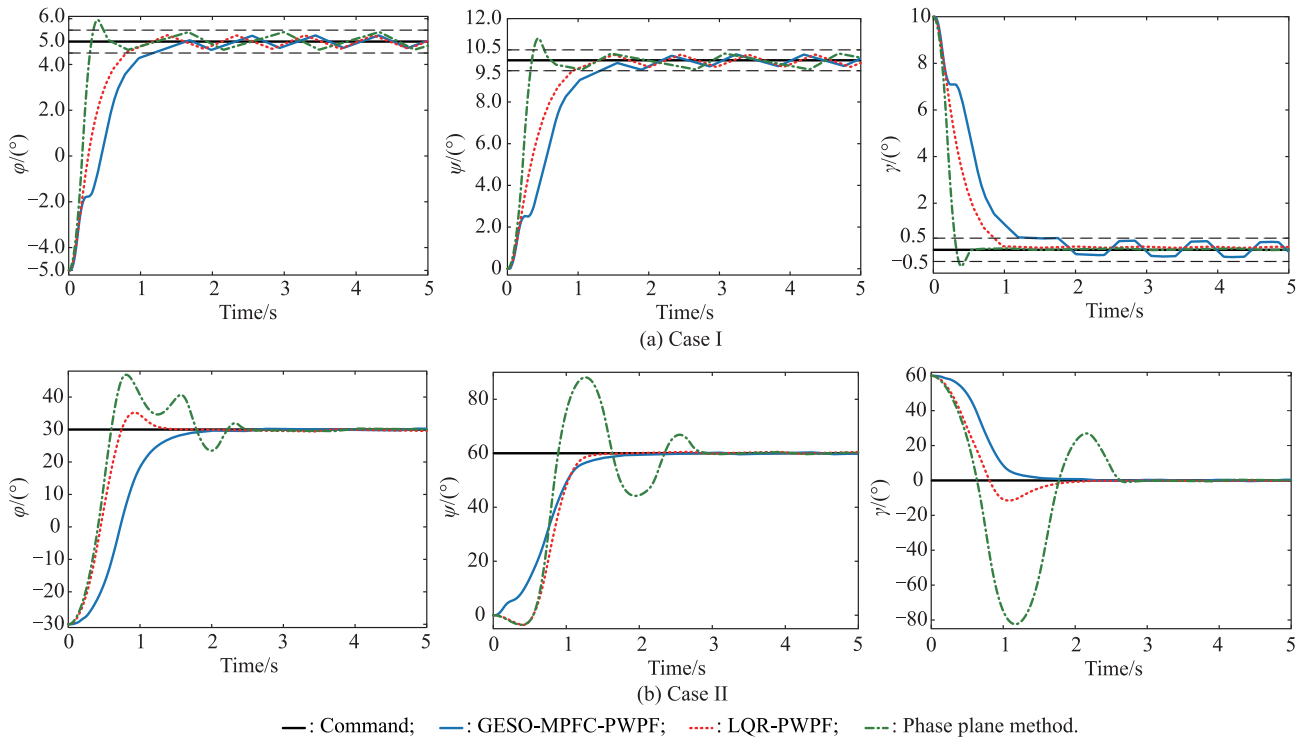


Fig. 5 Response curves for static tracking

5.3 Dynamic tracking

To further test the dynamic tracking performance of three controllers, sine signal with frequency of 0.1 Hz and 0.25 Hz are selected as reference command in Case I (slow angular slew) and Case II (fast angular slew) respectively. And the simulation results are depicted in Fig. 7 (response curves) and Fig. 8 (corresponding control command).

It is obvious from Fig. 7 that the response curves under

LQR-PWPF controller lag behind the reference command both in Case I and Case II. When performing slow angular slew maneuver, the response curves under GESO-MPFC-PWPF controller and phase plane controller almost overlap with reference command. When accelerating the sine signal frequency, the phase plane controller results in the response curves divergency, but after slightly adjusting in the first 2 s, the GESO-MPFC-PWPF controller precisely tracks the reference command.

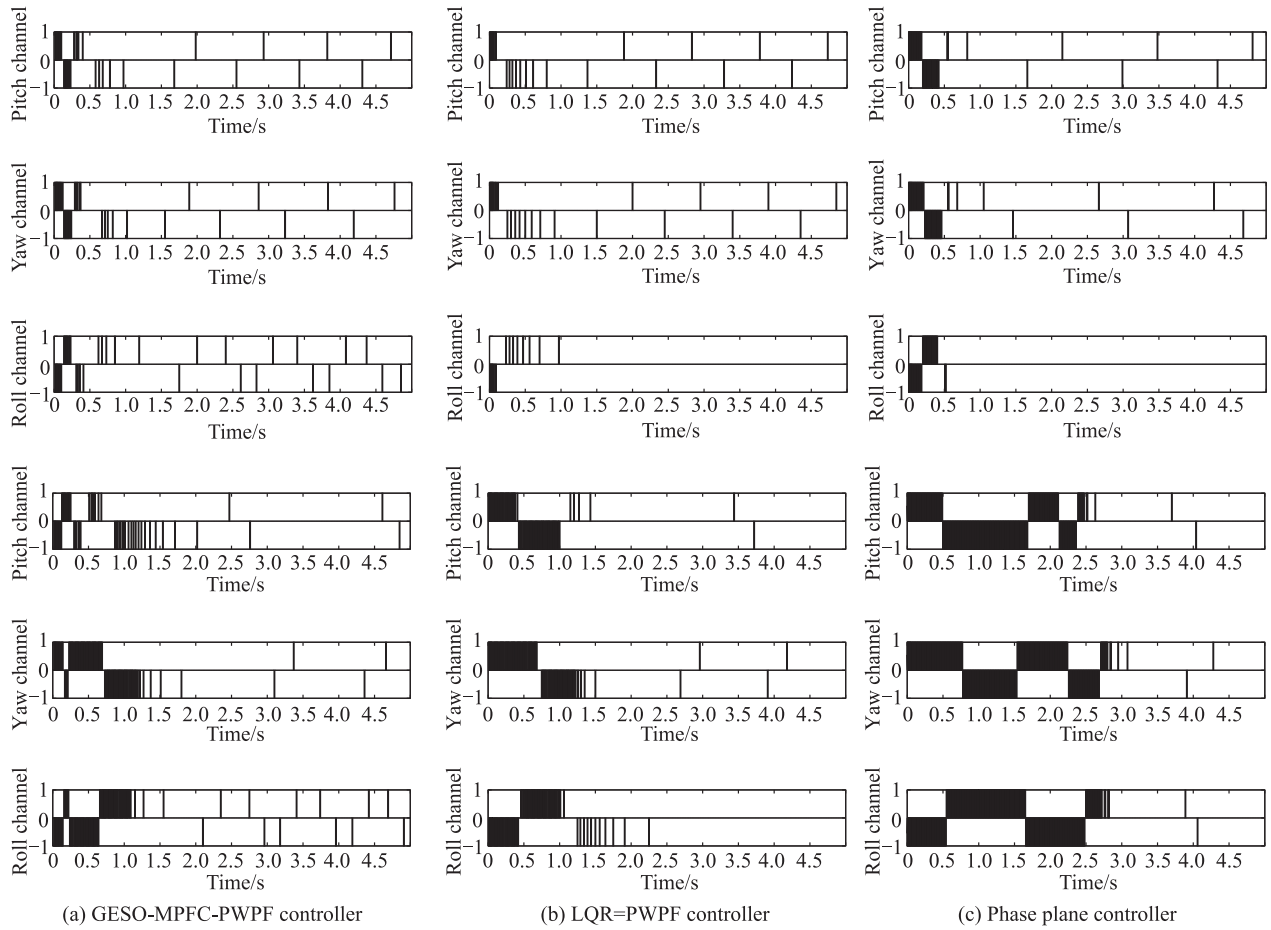


Fig. 6 Control command for static tracking in Case I (the first three rows) and Case II (the last three rows)

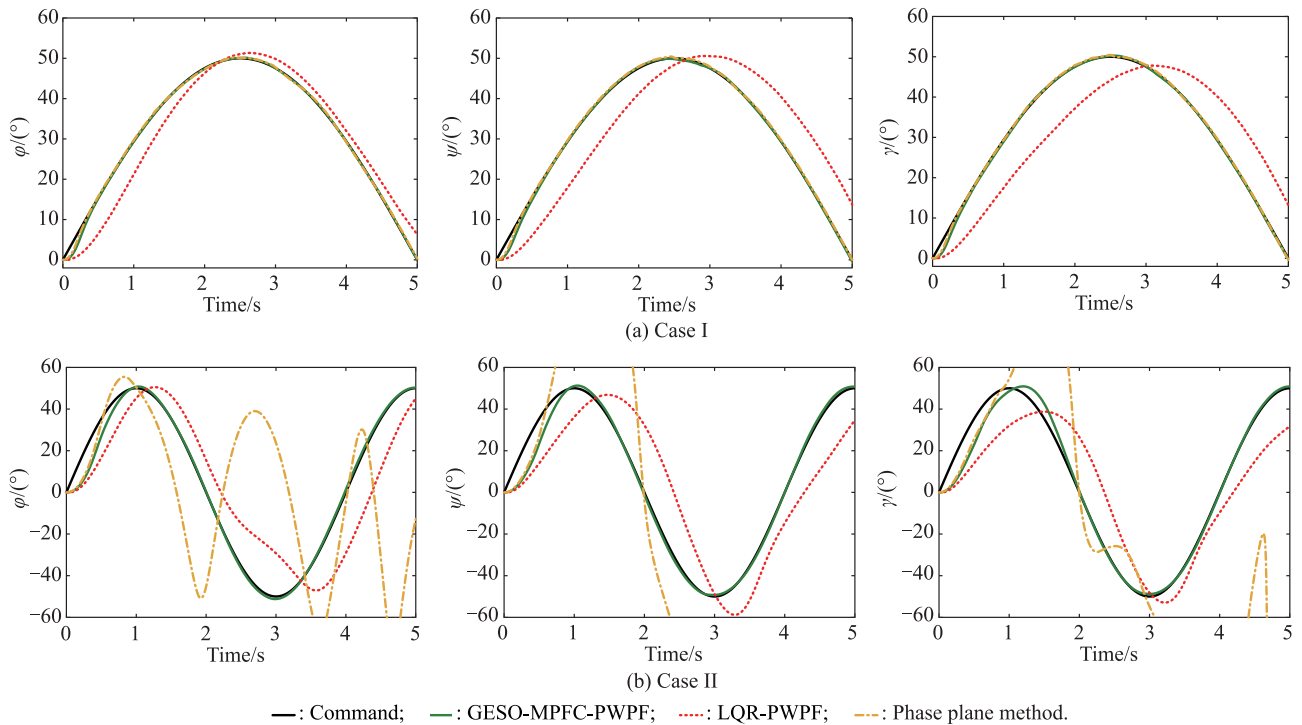


Fig. 7 Response curves for dynamic tracking

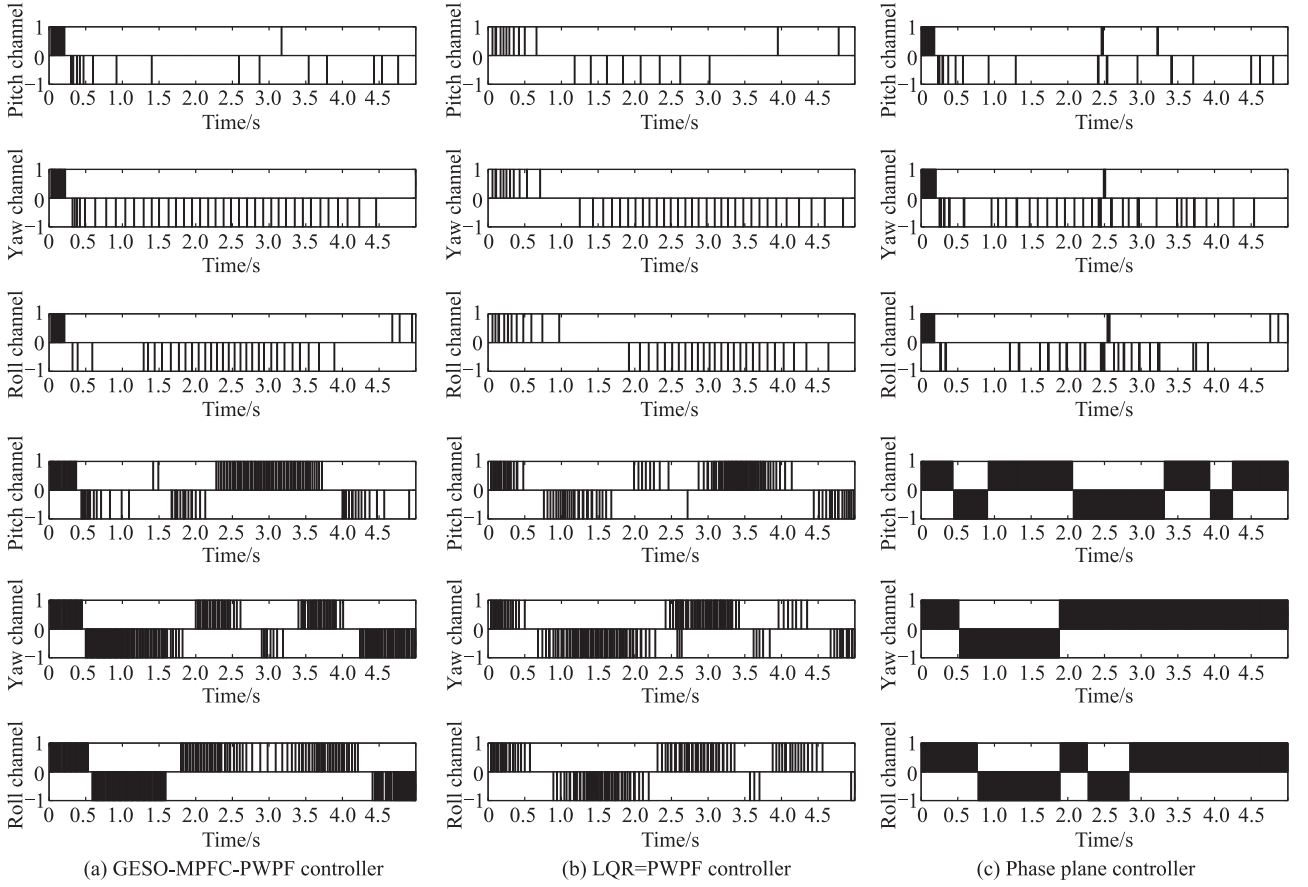
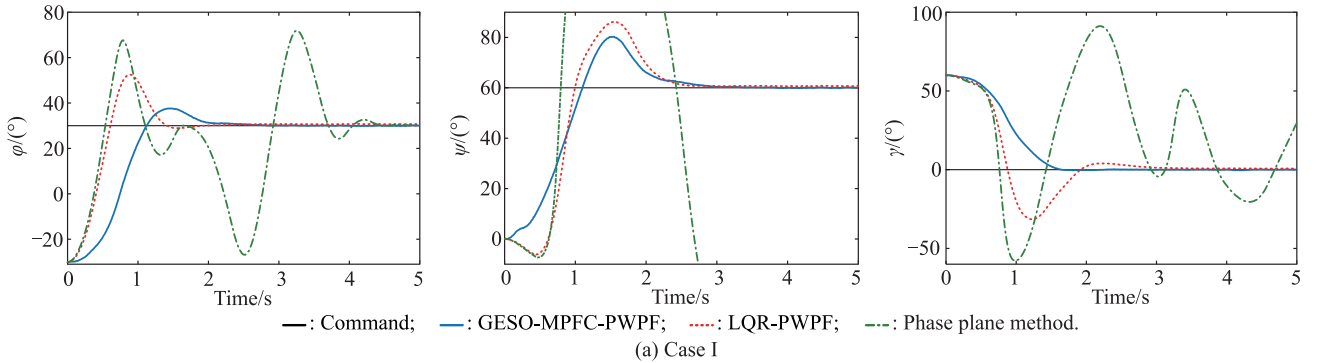


Fig. 8 Control command for dynamic tracking in Case I (the first three rows) and Case II (the last three rows)

5.4 Robustness testing

A more realistic scenario with measurement noise is considered in this case to test the robustness of three controllers. Herein, it is assumed that the moment of inertia and control moment increase 20% and 10% respectively. And suppose external disturbances are imposed on three control channels, which are assumed as one-tenth of the control moment, namely $\Delta M_x = 0.48 \text{ N} \cdot \text{m}$, $\Delta M_y = 0.874 \text{ N} \cdot \text{m}$, $\Delta M_z = 0.874 \text{ N} \cdot \text{m}$. Besides,

cross product of inertia is also added in this case ($\text{kg} \cdot \text{m}^2$), i.e., $I_{xy} = I_{yx} = 0.3$, $I_{xz} = I_{zx} = 0.4$, and $I_{yz} = I_{zy} = 0.5$. Moreover, a zero mean 0.001 rad standard deviation white noise with 10 ms sampling time and a zero mean 0.01 rad/s standard deviation white noise with 10 ms sampling time are supposed to interfere the measurement of the attitude angle and angular velocity respectively. Under above setting, the results for large angle maneuver (Case I) and fast angular slew (Case II) are presented in Fig. 9 and Fig. 10.



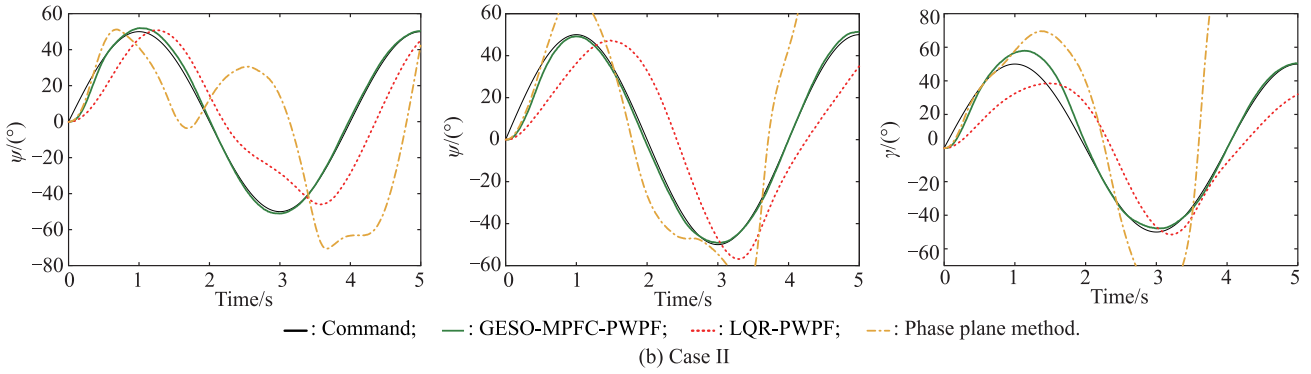


Fig. 9 Response curves for robustness test

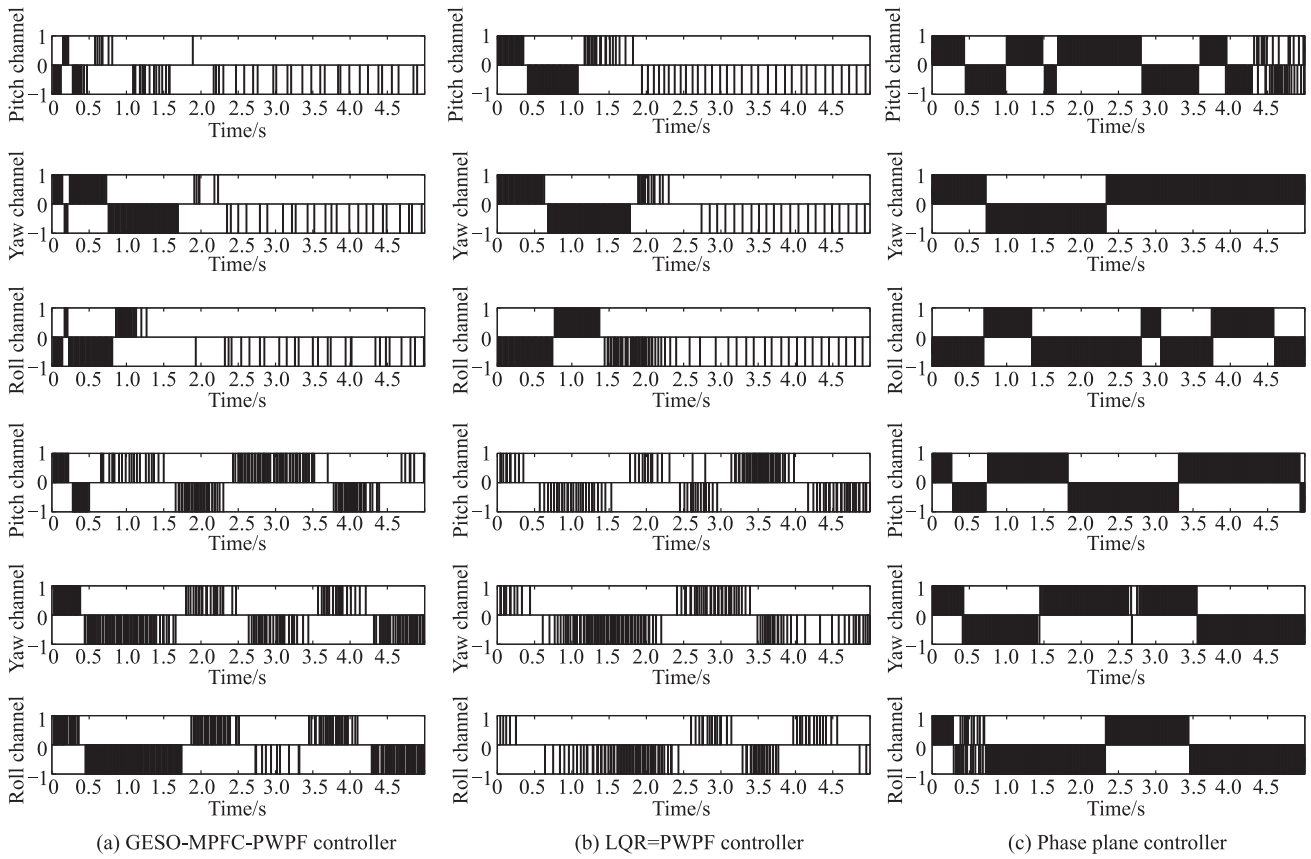


Fig. 10 Control command for robustness test in Case I (the first three rows) and Case II (the last three rows)

In Case I, the strong perturbations, disturbances and cross couplings lead to an obvious overshoot both for GESO-MPFC-PWPF controller and LQR-PWPF controller, while the overshoot for the former is always smaller than that of the later. And it is worth noting that the overshoot for GESO-MPFC-PWPF controller could be eliminated by decelerating the expected settling time T_r . For phase plane controller, the given setting is far beyond its control authority. The response curves for it in Case I obviously diverge, so does it in Case II. In same cases, the re-

sponse curves for LQR-PWPF controller still dramatically lag behind the reference command. Only GESO-MPFC-PWPF controller among them is capable of precisely tracking the rapid-varying sine reference signal. The satisfying performance for GESO-MPFC-PWPF controller both in Case I and Case II well demonstrates its strong robustness against perturbations and disturbances.

5.5 Fuel consumption

Fuel consumption is an important index to judge a con-

troller for RCS thrusters. For attitude fine-tuning in static tracking, Fig. 6 shows LQR-PWPF controller and phase plane controller both require less fuel consumption than that of GESO-MPFC-PWPF controller. However, for large angle maneuver, the fuel consumption obviously increases for the former two but remain unchanged for the later. According to Fig. 8, when performing dynamic tracking, phase plane controller consumes the highest fuel among three comparative controllers for response curve divergency, especially for fast angular slew. And from three simulation case results, it is obvious that perturbation case does not burden GESO-MPFC-PWPF controller with additional fuel consumption to reject severe disturbances and uncertainties compared to nominal cases. While the other two controllers, their fuel consumptions increase to a greater or less degree.

6. Conclusions and discussions

How to actively reject internal perturbations and external disturbances for space vehicles mounted on RCS is investigated in this paper and a dual-unit robust controller is proposed. Different from traditional robust control methodologies, this design not only accesses the strong robustness against above uncertainties without sacrificing the nominal or the best performance but also requires no additional fuel consumption. Rigorous and high-fidelity numerical simulations offer a convincing evidence of feasibility and superiority of this design in terms of precise tracking, satisfying dynamical character, and strong robustness even when large angle and/or fast angular slew maneuvers are performed.

References

- [1] MARTIN F H, BATTIN R H. Computer-controlled steering of the Apollo spacecraft. *Journal of Spacecraft and Rockets*, 1967, 5(4): 400–407.
- [2] SUN B C, PARK Y K, ROH W R, et al. Attitude controller design and test of Korea Space Launch Vehicle-I upper stage. *International Journal Aeronautical and Space Sciences*, 2010, 11(4): 303–312.
- [3] GILBERTO A J, LUIZ S M, SANTANA A C. Optimal on-off attitude control for the Brazilian multission platform satellite. *Mathematical Problems in Engineering*, 2009, DOI: 10.1155/2009/750945.
- [4] TING T, FIANAGAN N. Space shuttle transition controller OMS-TVC and RCS jet thruster stability analysis. *Proc. of the 27th AIAA/SAE/ASME/ASEE Joint Propulsion Conference*, 1991: 1–12.
- [5] CALHOUN P C, QUEEN E M. Entry vehicle control system design for the Mars science laboratory. *Journal of Spacecraft and Rockets*, 2006, 43(2): 324–329.
- [6] BROWN T. In-flight tuning of the Cassini RCS attitude controller. *Proc. of the AIAA Guidance, Navigation, and Control Conference*, 2011: AIAA 2011-6550.
- [7] DOMAN D B, GAMBLE B J, NGO A D. Quantized control allocation of reaction control jets and aerodynamic control surfaces. *Journal of Guidance, Control, and Dynamics*, 2009, 32(1): 13–24.
- [8] THURMAN S W, FLASHNER H. Robust digital autopilot design for spacecraft equipped with pulse-operated thrusters. *Journal of Guidance, Control, and Dynamics*, 1996, 19(5): 1047–1055.
- [9] JOHANSEN C T, DANEHY P M, ASHCRAFT S W, et al. PLIF study of Mars Science Laboratory capsule reaction control system jets. *Proc. of the 41st AIAA Fluid Dynamics Conference*, 2011: 27–30.
- [10] WENG L G, LI B, CAI W C, et al. Human memory/learning inspired approach for attitude control of crew exploration vehicles (CEVs). *Proc. of the American Control Conference*, 2007: 3843–3848.
- [11] CHIANG R, BRECKENRIDGE W, WONG E. Self-tuning thruster control for Cassini spacecraft. *Proc. of the AIAA Guidance, Navigation, and Control Conference*, 1996: AIAA 1996-3822.
- [12] SINGH T. Fuel/time optimal control of the benchmark problem. *Journal of Guidance, Control, and Dynamics*, 1995, 18(6): 1225–1231.
- [13] HABLANI H B. Multiaxis tracking and attitude control of flexible spacecraft with reaction jets. *Journal of Guidance, Control, and Dynamics*, 1994, 17(4): 831–839.
- [14] PARADISO J A. Adaptable method of managing jets and aerodynamic surfaces for aerospace vehicle control. *Journal of Guidance, Control, and Dynamics*, 1991, 14(1): 44–50.
- [15] KRØVEL T. Optimal tuning of PWPF modulator for attitude control. Trondheim, Norway: Norwegian University of Science and Technology, 2005.
- [16] CUI L, YANG Y. Disturbance rejection and robust least-squares control allocation in flight control system. *Journal of Guidance, Control, and Dynamics*, 2011, 34(6): 1632–1643.
- [17] GENG J, SHENG Y Z, LIU X D. Finite-time sliding mode attitude control for a reentry vehicle with blended aerodynamic surfaces and a reaction control system. *Chinese Journal of Aeronautics*, 2014, 27(4): 964–976.
- [18] RICHALET J. Industrial applications of model based predictive control. *Automatica*, 1993, 29(5): 1251–1274.
- [19] HE F H, MA K M, YANG B Q, et al. Model predictive control for a missile with blended lateral jets and aerodynamic fins. *Proc. of the 27th Chinese Control Conference*, 2008: 430–434.
- [20] BURCHETT B. Predictive optimal pulse-jet control for symmetric projectiles. *Proc. of the AIAA Atmospheric Flight Mechanics Conference*, 2014: AIAA 2014-0883.
- [21] LEOMANNI M, ROGERS E, GABRIEL S B. Explicit model predictive control approach for low-thrust spacecraft proximity operations. *Journal of Guidance, Control, and Dynamics*, 2014, 37(6): 1780–1790.
- [22] YANG W, BOYD S P. Fast model predictive control using online optimization. *IEEE Trans. on Control Systems Technology*, 2010, 18(2): 267–278.
- [23] MAALOUF A I. Improving the robustness of a parallel robot using predictive functional control (PFC) tools. *Proc. of the 45th IEEE Conference on Decision and Control*, 2006: 6468–6473.
- [24] ROSSITER J A, RICHALET J. Handling constraints with predictive functional control of unstable processes. *Proc. of the*

- American Control Conference, 2002: 4746–4751.
- [25] SATOH T, KANEKO K, SAITO N. Performance improvement of predictive functional control: a disturbance observer approach. Proc. of the IECON 37th Annual Conference on IEEE Industrial Electronics Society, 2011: 669–674.
- [26] LIU H X, LI S H. Speed control for PMSM servo system using predictive functional control and extended state observer. IEEE Trans. on Industrial Electronics, 2012, 59(2): 1171–1183.
- [27] ZHANG Y H, YANG H B, JIANG Z Y, et al. Robust predictive functional control for flight vehicles based on nonlinear disturbance observer. International Journal of Aerospace Engineering, 2015: 878971.
- [28] LI S H, YANG J, CHEN W H, et al. Generalized extended state observer based control for systems with mismatched uncertainties. IEEE Trans. on Industrial Electronics, 2012, 59(12): 4792–4802.
- [29] SHE J H, FANG M X, OHYAMA Y, et al. Improving disturbance-rejection performance base on an equivalent-input-disturbance approach. IEEE Trans. on Industrial Electronics, 2008, 55(1): 380–389.
- [30] HUNT L R, MEYER G, SU R. Noncausal inverses for linear systems. IEEE Trans. on Automatic Control, 1996, 41(4): 608–611.
- [31] LI T, ZHANG S F, YANG H B, et al. Robust missile longitudinal autopilot design based on equivalent-input-disturbance and generalized extended state observer approach. Proceedings of the Institution of Mechanical Engineers, Part G: Journal of Aerospace Engineering, 2015, 229(6): 1025–1042.
- [32] ANTHONY T C, WIE B, CARROLL S. Pulse-modulated control synthesis for a flexible spacecraft. Journal of Guidance, Control, and Dynamics, 1990, 13(6): 1014–1022.
- [33] XU X Y, CAI Y L. Pulse-width pulse-frequency based optimal controller design for kinetic kill vehicle attitude tracking control. Applied Mathematics, 2011, 2(5): 565–574.

Biographies



TIAN Jiayi was born in 1990. He received his B.S. degree and M.S. degree in aeronautical and astronautical science and technology from Beihang University and National University of Defense Technology in 2013 and 2015 respectively. He is now pursuing his Ph.D. degree in National University of Defense Technology. His research interests include disturbance rejection based control and aircraft dynamics and control.

E-mail: tianjy618@hotmail.com



ZHANG Shifeng was born in 1971. He received his Ph.D. degree in control theory and engineering from National University of Defense Technology in 2000. His research interests cover aircraft overall design, flight dynamics, guidance and control, inertial navigation, and measurement and precision analysis. He is currently a Fellow of the Unmanned Aerial Vehicle System Engineering and Flight Test Committee, a Fellow of the Chinese Society of Astronautics Aircraft Overall System Committee, and Topic Principal of the 973, 863 Project Management Office.

E-mail: zhang_shifeng@hotmail.com